A. Sanz and J. M. Perales

Liquid Bridge Formation

The formation of a liquid bridge is obviously the first step in the experimentation of the different aspects of the liquid bridge dynamics. Among the several candidate procedures of formation the authors have selected the so called "cylindrical formation": liquid is injected inside of the bridge through one of the supporting disks whereas simultaneously one of the disks is moved apart from the other at the proper speed to keep the volume of liquid inside the column, the same that of the cylinder limited by both disks. Besides its own fluid mechanics interest (interplay between a jet and an interface), the results of this study would be very useful for experimenters in order to reduce the experiment preparation phase, as the total time allowed is scarce in most often used reduced gravity facilities (parabolic flights, sounding rockets and so on). A simplified theoretical model of the problem is presented which is valid in a flow regime limited in range by the Reynolds number of the injection jet. The existence of contiguous regimes and the influence of Ohnesorge number are suggested. This characterization has been deduced from the experiments performed by using the neutral buoyancy technique on earth and helps to explain the behaviour observed during experiments performed on microgravity conditions onboard sounding rockets (TEXUS).

1 Introduction

The aim of this paper is to analyze the formation of a liquid bridge, which is performed by the axial injection of fluid inside of the liquid bridge through one of the disks while the disks are simultaneously separated at constant speed. This subject has been previously experimentally studied [1] and the main points outlined were the following ones:

a) the most interesting process is the filling which could give rise to the breaking of the bridge, whereas the removal of the liquid has minor influence in the deformation of the interface;

b) during the injection there are at least two main different deformation modes which suggests the existence of two different and competing driving mechanisms.

From a theoretical point of view, the complete analysis of the problem requires the solution of the Navier-Stokes equations with boundary conditions at a moving boundary (moving disks) and at free boundary (the interface). To the authors' knowledge this is an untreated problem, although there are a large amount of studies on more simple configurations. One of the basic configurations receiving more attention is the jet discharge in an infinite or semi-infinite medium at low Reynolds numbers, $R = 2\ R_i\ V_i/\nu_i$, where R_i is the injection hole radius, V_i the mean speed of injection and ν_i the kinematic viscosity of the liquid of the bridge.

These studies can be summarized as follows: *Schade* (1958) in an unpublished paper and *Viilu* [2] dealt with the experimental determination of the Reynolds number at which the jet becomes unstable. *Reynolds* [3] described the instability shapes and introduced the concept of laminar length, which is the distance from the injection hole to the point where instability appears. *McNaughton* and *Sinclair* [4] performed experiments in the range $100 < R < 28{,}000$ to determine the laminar length in the coaxial discharge of a jet inside a cylindrical container which is evacuated from the opposite end. Disregarding the effect of interface deformation, this is perhaps the configuration more similar to that studied here although in a larger Reynolds number range.

From the literature revisited, several conclusions can be pointed out:

a) Jet formation and penetration length.

From the experiments of *Taylor* [5], no jet is formed at $R = 0.05$, and a short jet of roughly 3 diameter length, ending in a moushroom-like shape, appears at $R \approx 10$, whereas at $R = 200$ the jet reachs the opposite wall, some 60 diameters apart. These experiments correspond to the starting of injection.

The analytical study of the transient starting of a jet in an infinite medium [6] shows that the formation of a jet appears when $R > 27$ ($R_c > 6$, $R_c = \pi^{1/2} \cdot R/8$ is the Reynolds number used in that paper). Another study [4] shows that in the regime $R < 300$ called "dissipated laminar jet", the jet penetrates in the surrounding fluid a distance D, which can be fitted by the expression $D/R_i \approx 47 \cdot \log R - 90$ ($100 < R < 300$), so that for $R = 100$, $D/R_i \approx 4$.

b) Influence, of temperature difference between the jet and the surrounding fluid.

The above correlation between D and R is a rough fitting, the experimental data [4] being largely dispersed due to the large influence of buoyancy in this regime ($R < 300$).

A detailed analysis of this effect can be found in [7]. Concerning the injection in the liquid bridge, if there are some temperature difference between the liquid in the reservoir and in the bridge, this phenomenon will have some importance only in the first trials during which the fluid in the reservoir would become mixed with that in the bridge.

c) Formation of a recirculation vortex around a jet impinging against a wall.

The numerical analysis of the jet discharging from a tube against a wall [8] shows that a recirculation vortex appears for $R < 100$ (in this case the wall is placed $4R_i$ apart from the injection hole). As R increases the vortex moves outside the observation frame. In the liquid bridge configuration the jet is confined, so it is possible that the vortex remain near

Mail address: Dr. A. Sanz, Lab. Aerodinámica, E.T.S.I. Aeronáuticos, Universidad Politécnica de Madrid, E-28040 Madrid, Spain.

the opposite disk for large values of R. From the observation of the streamlines in that paper it can be deduced that a jet-like flow appears at $R \approx 25$ (result similar to that in [6]), and for $R > 100$ the nature of the flow do not change, being essentially the same as at $R = 1000$. Turbulence does not arise because of the characteristics of the numerical model.

Concerning this study, in section 2 some theoretical analysis are presented which help both to reduce the number of variables in the problem and to explain the experimental results; section 3 contains a summary description of the experiment set-up, the trials performed and the data processing; in section 4 the main results are presented, and section 5 collects main conclusions.

2 Theoretical Analysis

The first attempt is to perform a dimensional analysis of the problem. The geometry and main features of the problem are shown in fig. 1. Neglecting gravity forces the parameters which characterize the problem are:

- Geometry: disk radius, R_0; disk separation, L; injection radius, R_i
- Kinematic: disk separation speed, V_d; injection speed, V_i
- Fluid properties: bridge liquid density, ϱ_i; surrounding liquid density, ϱ_0; viscosities, ν_i and ν_0, respectively.
- Interface properties: interface tension, σ.

Concerning the position of the three-phases contact line the interface is supposed to be anchored to the disks edge so that the contact angle do not play a role. The shape of the interface is given by the expression

$$F(z,t) = F(z,t,L,R_0,\ R_i,V_d,V_i,\nu_i,\nu_0,\varrho_i,\ \varrho_0,\sigma)$$

With the aid of the dimensional analysis concepts it can be reduced in the form

$$F(Z,T)/R_0 = G(Z,\ T,\ \Lambda,\ \alpha,\ R,\ W,\ St,\ \nu,\ \varrho)$$

where

$Z = z/R_0$ is the dimensionless axial coordinate,
$T = t/t_c$ is the dimensionless time ($t_c = L/V_d$ is the characteristic time of the experiment),
$\Lambda = L/(2\ R_0)$ is the slenderness of the liquid bridge,

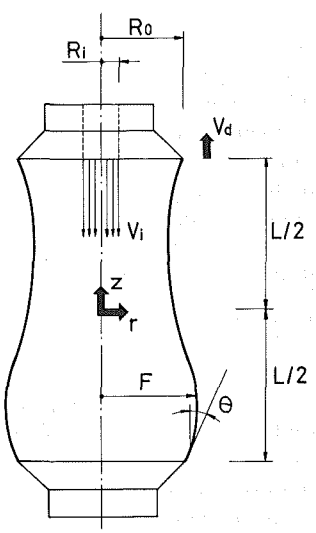

Fig. 1. Geometry and coordinate system for the liquid bridge injection configuration

$\alpha = R_i/R_0$ is the radius ratio,
$W = \varrho_i\ V_d^2\ R_0/\sigma$ is the Weber number,
$St = t_r/t_c = V_d/V_i$ is the Strouhal number ($t_r = L/V_i$ is the residence time), and
$\nu = \nu_0/\nu_i$ and $\varrho = \varrho_0/\varrho_i$ are the viscosity and density ratios, respectively.

The parameters ν and ϱ are defined by the experimental configuration. In neutral buoyancy $\nu \approx \varrho \approx 1$ in most cases, and the influence of these parameters remain the same.

Roughly speaking the formation and penetration of the jet would be driven by R, the formation and position of the recirculation vortex by R and Λ, and the interaction between the jet and the interface by R, α, W and Λ.

Aiming at to simplify the interpretation of the data obtained in the experiments a simple theoretical model has been developed, based on the following assumptions:

(1) The flow is axisymmetric, and pressure is constant across every section of the liquid bridge.
(2) The motion is almost-steady during most of the formation, and time appears only as a parameter. This is based on the value of St, which is generally $St \ll 1$ so that the residence time is much smaller than the characteristic time. The normal speed at the interface should be much smaller than the mean injection speed, V_i.
(3) Viscous effects at the interface are neglected.
(4) In the neutral buoyancy experiments, $\varrho = 1$. This is a substantial difference with the case of microgravity.
(5) Physical properties are considered constant.
(6) No vortex effects are considered.

The disk speed, V_d, is constant, as it occurs in a typical experiment, and the injection rate is the appropriate one to maintain the volume of the bridge equal to that of a cylinder with radius R_0 and length L.

By using the conservation of mass and momentum in a control volume which is fixed in time and coincides at a given instant with the position of the disks and the interface, in a reference system fixed to the injection disk the following expressions can be obtained

$$V_i = V_d/\alpha^2 \tag{1}$$

$$\varrho_i(V_i^2\ R_i^2 - V_d^2\ R_0^2) = \Delta p\ R_0^2 + F_s/\pi \tag{2}$$

where

Δp is the pressure difference between the disks, and
F_s is the axial force which the interface generates over the fluid,

$$F_s = 2\,\pi \int_{-L/2}^{L/2} p_i(z)\ F_s(z)\ F'(z)\,\mathrm{d}z \tag{3}$$

where

p_i is the pressure inside the liquid bridge, and
prime denotes differentiation respect to z.

In (1) and (2) the mass and momentum flows across the part of the control volume that coincides with the interface have been neglected according to assumption (2).

The normal pressure jump across the interface gives

$$p_i(z) - p_0 = \sigma\ C(z) \tag{4a}$$

where

p_0 is the pressure outside the liquid bridge.

The hydrostatic pressure is not considered in p_i and p_0 because its jump accross the interface is null in the case $\varrho = 1$.

$C(z)$ is the mean curvature which can be stated as follows

$$C(z) = \frac{1}{F}\frac{\mathrm{d}}{\mathrm{d}F}\left(\frac{F}{(1 + F'^2)^{1/2}}\right) \tag{4b}$$

Combining expressions (4a) and (4b), the integration in (3) can be performed

$$F_s = 2\,\pi\,\sigma\,R_0[\cos\,\theta(L/2) - \cos\,\theta(-\,L/2)] \tag{5}$$

where

$\theta(z)$ is the angle between the slope of the interface and the z-axis.

For small deformations of the interface, F_s can be neglected in comparison with the other terms in (2) so that the momentum of the jet gives rise mainly to a pressure difference at the disks.

The interface would be deformed by the pressure field generated by the jet. Following this simplifying way, the pressure field can be considered as a linear variation between the extreme values at the disks Δp which can be deduced from (1) and (2)

$$\Delta p = \varrho_i\,V_d^2\,(1 - \alpha^2)/\alpha^2 \tag{6}$$

The deformation of the interface under a linear axial variation of the pressure has been studied in the case of a liquid bridge subjected to an axial gravity [9]. According to this reference, the pressure difference at the disks can be expressed in the following dimensionless form

$$B = \Delta p\,R_0/(2\,\Lambda\,\sigma) \tag{7}$$

where

B (Bond number) represents the ratio between the imposed pressure difference and the capillary pressure jump. In the case of the pressure gradient generated by the injection jet, the suitable Bond number results from the substitution of Δp given by (6) in (7), that is

$$B = W(1 - \alpha^2)\,(2\,\Lambda\,\alpha^2)^{-1} \tag{8}$$

The dimensionless interface deformation, $f = F/R_0 - 1$, under a linear pressure field is given by [9]

$$f(Z) = B\left(Z - \frac{\Lambda}{\sin\,\Lambda}\sin\,Z\right) \tag{9}$$

The deformation in (9) is antisymmetric with respect to $Z = 0$ which is consistent with the assumption $F_s = 0$. The largest deformation of the interface, $f = f_m$, occurs at $Z = Z_m$

$$Z_m = \cos^{-1}(\sin\,\Lambda/\Lambda) \tag{10}$$

Thus, f_m can be seen as the product of an excitation factor, B, and a modulator factor which depends on Λ, although B depends also on Λ as the pressure gradient between the disks depends on their separation.

The dimensionless numbers above can be related in the following form

$$R = \frac{2}{\alpha}\frac{W^{1/2}}{Oh} = \left(\frac{8\,\Lambda}{1 - \alpha^2}\right)^{1/2}\frac{B^{1/2}}{Oh} \tag{11}$$

where

$Oh = \nu_i\,(\sigma\,R_0/\varrho_i)^{-1/2}$ is the Ohnesorge number.

The first equality results from the definition of R and the second by using (8). For the values in the experiments which are presented in section 3 ($\sigma = 1.7\cdot10^{-2}$ Nm^{-1}, $\nu_i = 2\cdot10^{-5}$ m^2 s^{-1}, $\varrho_i = 954$ kgm^{-3}, $R_0 = 1.5\cdot10^{-2}$ m) one obtains $Oh \approx 4\cdot10^{-2}$ and for $\Lambda = 2$, with $\alpha \ll 1$ gives $R \approx 100\,B^{1/2}$. Oh only depends on the configuration (physical properties of liquids and geometry) and not on the operation (disk speed).

3 Experiment Description and Data Processing

In the experiments performed on earth the neutral buoyancy technique was used. In this technique the bridge is surrounded by another liquid immiscible with the liquid of the bridge and of equal density. The experimental set-up is shown in fig. 2. The main part of the apparatus is the *L*iquid *C*olumn *C*ell (LCC). This is the experimental facility used to perform experiments on board the sounding rocket TEXUS [1]. This apparatus has to be modified to allow for the containment of the surrounding liquid and to avoid the contact of this liquid with some parts of the LCC.

The liquid for the bridge was a silicone oil (DMS 20) of density, $\varrho_i = 954$ kg·m^{-3} and viscosity, $\nu_i = 2\cdot10^{-5}$ m^{2}s^{-1}.

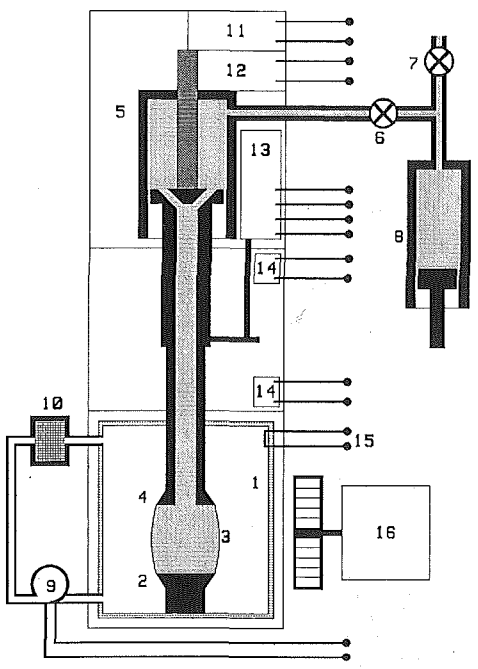

Fig. 2. Sketch of experimental setup with the LCC PTM (Liquid Column Cell-Plateau Tank Modification).
1) test chamber; 2) fixed disk; 3) liquid column; 4) injection disk; 5) syringe; 6) external feeding valve; 7) purge valve; 8) external syringe for maneouvre; 9) bath circulation pump; 10) filter; 11) tachometer generator; 12) syringe motor; 13) disk position transducer; 14) limit switches; 15) temperature sensor; 16) elapsed time and run number display

A few experiments were performed with oil of $5 \cdot 10^{-6}$ $m^2 s^{-1}$ viscosity (DMS 5). The surrounding liquid was a mixture (water and methanol) with the same density as the oil. The interface tension between the oil and the mixture was $\sigma = 1.7 \cdot 10^{-2}$ Nm^{-1}. Both disks were of 15 mm external radius, and trials were performed with disks with 2, 3 and 6 mm injection hole radii.

The experiment sequence, both in experiments on earth and in microgravity [1], consisted of the formation of a liquid bridge of cylindrical volume (injection of liquid and simultaneous disk separation) at several constant speeds aiming at to determine the largest possible speed which preserves the integrity of the bridge. Details on experiment preparation can be found elsewhere [10, 11].

The first formation in each sequence was performed at a speed slow enough so no interface deformation appear. The shapes obtained served as a guarantee or as a correction (if the deformation was not small enough) of the shapes obtained in the subsequent formations of the sequence.

Each sequence was filmed by a video camera and recorded by a video tape recorder. A LED display served to engrave the images with time and sequence marks. The sequences were automatically performed and controlled by a computer. The experiments performed are summarized in table 1. The retrieval speed was kept constant at 4.0 mm/s.

Data processing was as follows. Several pictures were taken from each sequence by means of a video copy processor (*Mitsubishi P70U*). Measurements of disk position and interface deformation were obtained from these pictures. Due to resources constraints and large quantity of images the decision was made to analyze only the most significant characteristics (and also the most simple) which is the neck width of the bridge, as a representative measurement of interface deformation. Some other reference measurements were also obtained to correct the image from distortions.

4 Results

The neck deformation, with respect to the cylinder, as a function of the bridge length, for several values of the disk speed and injection hole radius, is shown in fig. 3.

The same results but grouped as a function of Reynolds number, R, are plotted in fig. 4. Although a general behavior can be extracted - as R increases the deformation also increases - this parameter does not unify the results.

The variation of the amplifying factor (f_m/B, deformation to pressure gradient ratio) with the bridge slenderness Λ is shown in fig. 5. In these variables, experimental data are more tightly grouped with exception of large deformations or low R values. The theoretical value obtained by using expres-

Table 1. Experiments performed. Λ, maximum slenderness achieved (approx.); V_d, moving disk speed; R_i, injection hole radius; DMS X, silicone oil with viscosity X centistokes

		R_i = 3 mm	DMS 20			R_i = 2 mm	DMS 20
Num.	Λ	V_d [mm/s]	Comments	Num.	Λ	V_d [mm/s]	Comments
1	1.0	2.5,5.0	PT	34	2.3	1.0	
2	1.5	2.0,3.0	PT	35	1.0	6.0,7.0,8.0	
3	1.8	1.0,2.0,3.0	PT	36	1.0	8.0,9.0	
4	1.8	4.0,5.0,6.0	PT	37	1.5	1.0,7.0,8.0,10.0	A
5	2.0	2.0,3.0,4.0	PT	38	1.5	10.0,11.0	A, B
6	2.4	1.0,1.5,2.0	PT	39	2.0	1.0,2.0,4.0	A, B
7	2.4	2.5,3.0,3.5	PT	40	2.4	1.0,2.0,3.0	DD
8	2.6	1.0,1.5,2.0	PT	41	2.4	1.0,2.0,3.0	
9	2.6	2.5,3.0,3.5	PT	42	2.6	1.0,2.0,2.5	DD
10	1.0	2.0,8.0	A	43	2.6	1.0,2.0,2.5	DD
11	1.5	2.0,8.0	A	44	2.6	1.0,2.0,2.5,3.0	A, B
12	2.0	2.0,5.0	A	45	2.6	1.0,2.0,2.5,3.0	
13	2.4	2.0,4.0	A	46	2.8	0.5,1.0,2.5,3.0	
14	2.6	2.0,3.5,4.0	A	47	2.8	1.0	
15	1.0	2.0,9.0		48	2.8	1.0,1.5	
16	1.5	2.0,8.0					
17	2.0	2.0,5.0					
18	2.4	2.0,4.0	PT, DD, B				
19	2.4	2.0,4.0	DD, B				
20	2.6	2.0,3.0,3.5,4.0	DD				
		R_i = 6 mm	DMS 20			R_i = 2 mm	DMS 5
Num.	Λ	V_d [mm/s]	Comments	Num.	Λ	V_d [mm/s]	Comments
21	1.0	2.0,10.5	A	49	1.0	5.0,4.5	
22	1.5	2.0,11.0		50	1.5	2.0,4.0,3.5	
23	2.0	2.0,8.0,10.0	A, B	51	2.0	1.0,2.0,3.0,4.0	
24	2.4	2.0,7.0	DD	52	2.4	1.0,2.0,2.5	
25	2.4	2.0,7.0		53	2.6	1.0,2.0	
26	2.6	2.0,5.0,6.0,7.0	A, B				
27	1.0	2.0,9.5		Comments:			
28	1.5	2.0,8.5					
29	2.0	2.0,10.0	DD, B	PT,	preparatory trials without detailed data		
30	2.0	2.0,10.0,9.5	A	DD,	appreciable density differences		
31	2.6	2.0,7.0	B	B,	liquid bridge breaks		
32	2.7	2.0,7.0	DD, B	A,	analyzed sequence		
33	2.8	2.0,7.0,8.0	A, B				

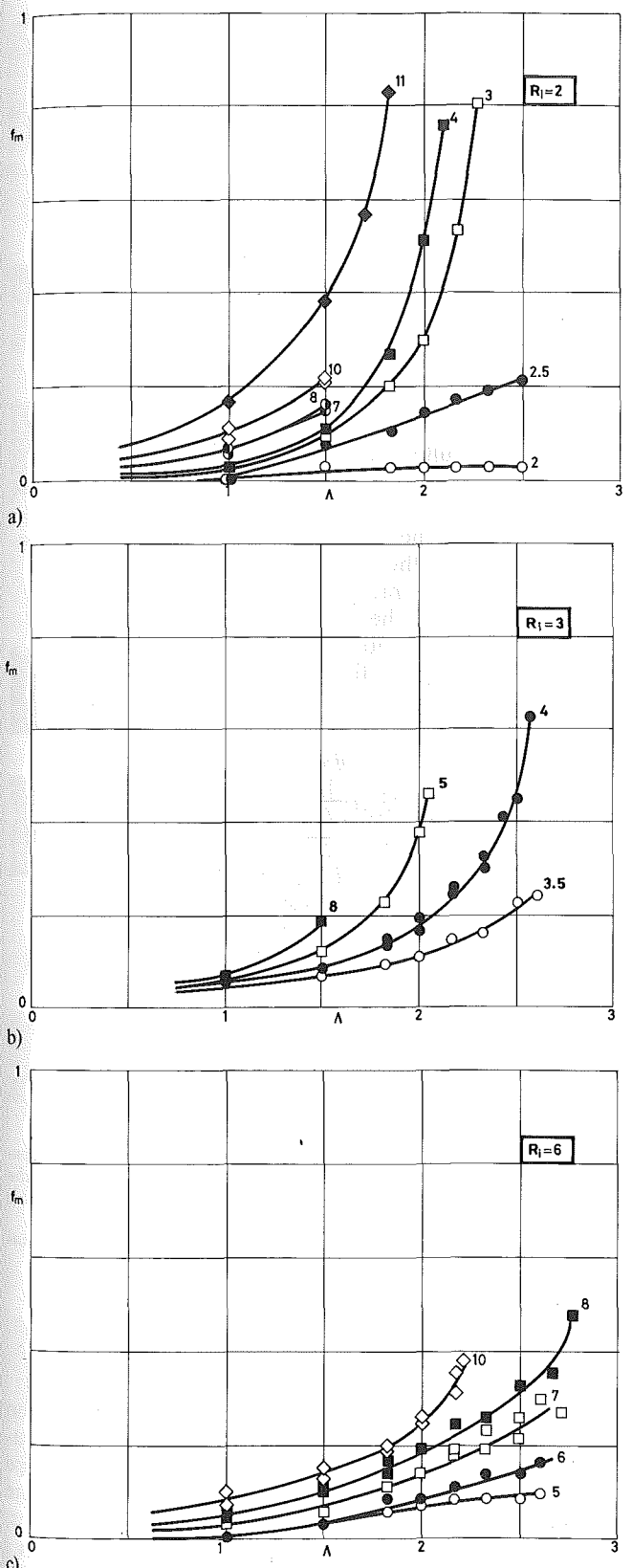

Fig. 3. Variation of the dimensionless deformation (with respect to the cylinder) of the liquid bridge neck, f_m, with the slenderness of the bridge, Λ, for several values of the injection hole radius, R_i
a) $R_i = 2$ mm; b) $R_i = 3$ mm; c) $R_i = 6$ mm. Figures indicate the injection disk speed in mm/s. Oh $\approx 4 \cdot 10^{-2}$

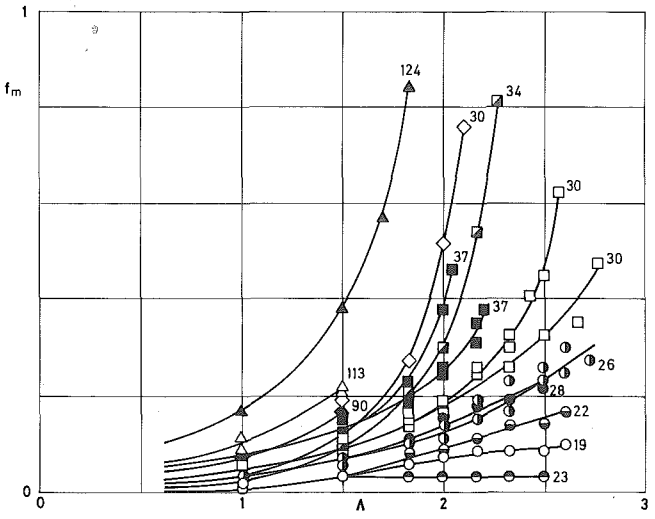

Fig. 4. Variation of the dimensionless deformation (with respect to the cylinder) of the liquid bridge neck, f_m, with the slenderness of the bridge, Λ, for several values of the Reynolds number, R, according to the following code: ○, 19; ◒, 22; ◓, 23; ◑, 26; ●, 28; □, 30; ◪, 34; ■, 37; ◇, 45; ◈, 60; ◆, 90; △, 113; ▲, 124. Oh $\approx 4 \cdot 10^{-2}$

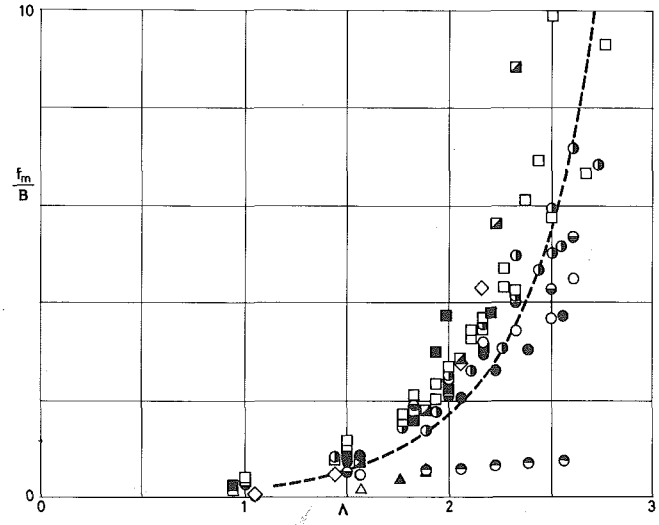

Fig. 5. Variation of the slenderness of the bridge, Λ, of the amplification factor, f_m/B, where f_m is the deformation and B (the Bond number) represents the imposed pressure gradient. Symbols represent the value of the Reynolds number, R, according to the following code (the same as in fig. 4): ○, 19; ◒, 22; ◓, 23; ◑, 26; ●, 28; □, 30; ◪, 34; ■, 37; ◇, 45; ◈, 60; ◆, 90; △, 113; ▲, 124. Dashed line: theoretical value obtained by using (9) and (10). Oh $\approx 4 \cdot 10^{-2}$

sions (9) and (10) multiplied by a matching factor ($k = 2$), is also plotted, showing a good agreement. The factor $k = 2$ represents the influence of the deviation of hypothesis introduced from the real situation: linear axial variation of pressure, almost-steady process, flat injection profile, etc.

On the other hand, as the interface evolution near the breaking is mainly driven by surface tension, the final evolution in all the breaking process should be alike, although slightly affected by other parameters. Thus, the variation of neck deformation as a function of Λ/Λ_c is shown in fig. 6 (Λ_c

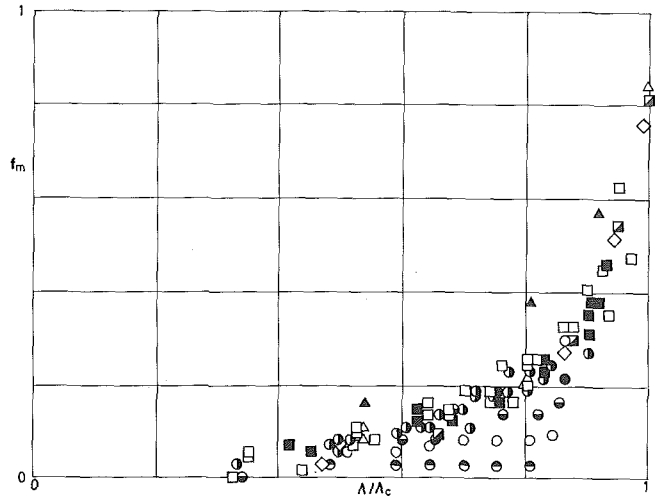

Fig. 6. Variation of the deformation, f_m, of the neck with the slenderness of the bridge, Λ. Λ_c is the value of Λ at which breaking occurs (at constant disk speed). Symbols represent the value of the Reynolds number, R, according to the following code (the same as in fig. 4): ○, 19; ◒, 22; ◓, 23; ◑, 26; ●, 28; □, 30; ◪, 34; ■, 37; ◇, 45; ◈, 60; ◆, 90; △, 113; ▲, 124. Oh ≈ $4 \cdot 10^{-2}$

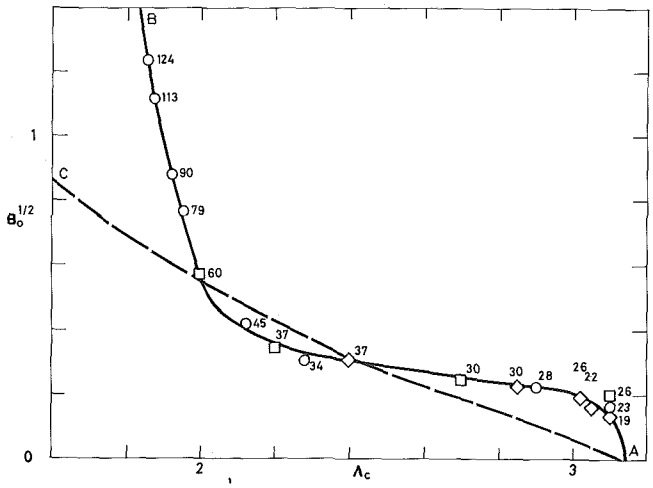

Fig. 7. Bond number, B (related in some range of Oh and Re with the pressure gradient imposed by the jet), which produces the breaking of the liquid bridge when the bridge reaches the slenderness Λ_c during a formation at constant speed (solid line). Stability limit of a liquid bridge under a constant and steady pressure gradient (dashed line). Figures indicate the Reynolds number, R. Symbols represent the injection hole radius, R_i: ○, R_i = 2 mm; □, R_i = 3 mm; ◇, R_i = 6 mm. Oh ≈ $4 \cdot 10^{-2}$

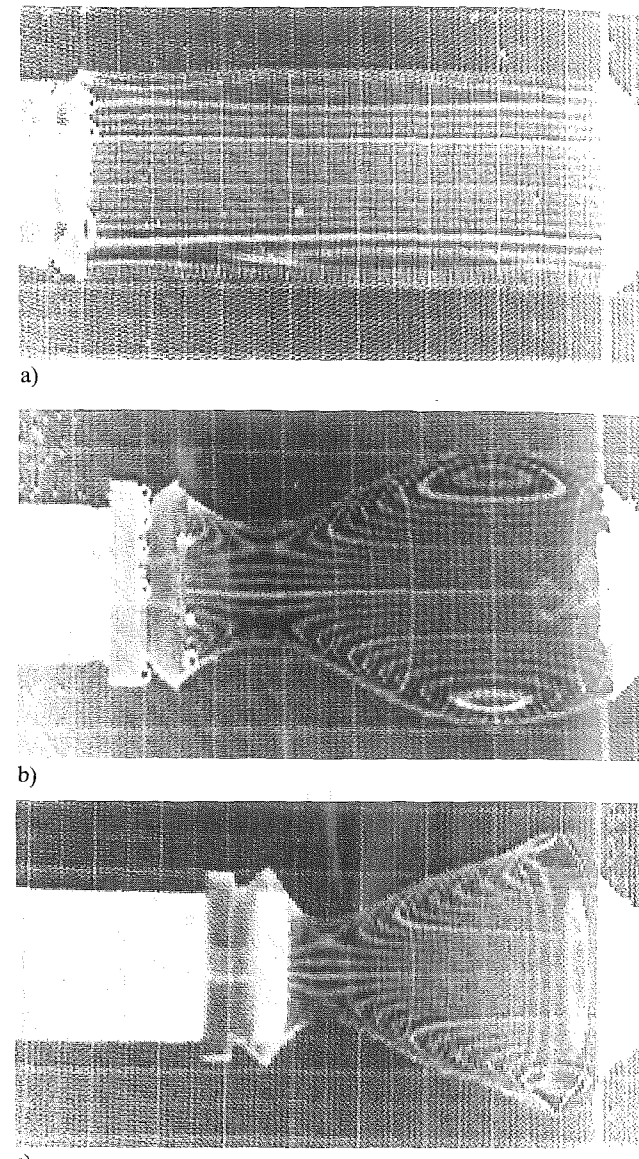

Fig. 8. Copies of video images taken during formation processes at constant speed. These picaures correspond to the latest stages, near the breaking, of three formations. R, Reynolds number. R_i, injection hole radius, R_i (mm)
a) R = 19, R_i = 6; b) R = 37, R_i = 3; c) R = 124, R_i = 2. The injection hole is in the moving disk (on the left).
Oh ≈ $4 \cdot 10^{-2}$

Table 2. Critical slenderness, Λ_c, at constant injection disk speed, V_d [mm/s] for several values of the injection hole radius, R_i [mm]

$R_i = 2$		$R_i = 3$		$R_i = 6$	
V_d	Λ_c	V_d	Λ_c	V_d	Λ_c
2	3.1	3.5	3.1	5	3.1
2.5	2.9	4	2.7	6	3.05
3	2.28	5	2.2	7	3.02
4	2.12	8	2.0	8	2.85
7	1.95			10	2.4
8	1.92				
10	1.87				
11	1.85				

is the slenderness of the bridge at the breaking in a formation process at constant speed). Λ_c has been determined straightforwardly in the formation processes ending in a breakage and by evolution fitting otherwise (table 2). In fact, all the evolutions, except those with small R or large deformations, show a similar behavior.

The previous results allow one to define a stability limit AB in the plane B-Λ which defines the maximum constant speed allowed for setting up a liquid bridge of a given length (and cylindrical volume), as shown in fig. 7. In this figure is presented also the stability limit AC of a liquid bridge (of cy-

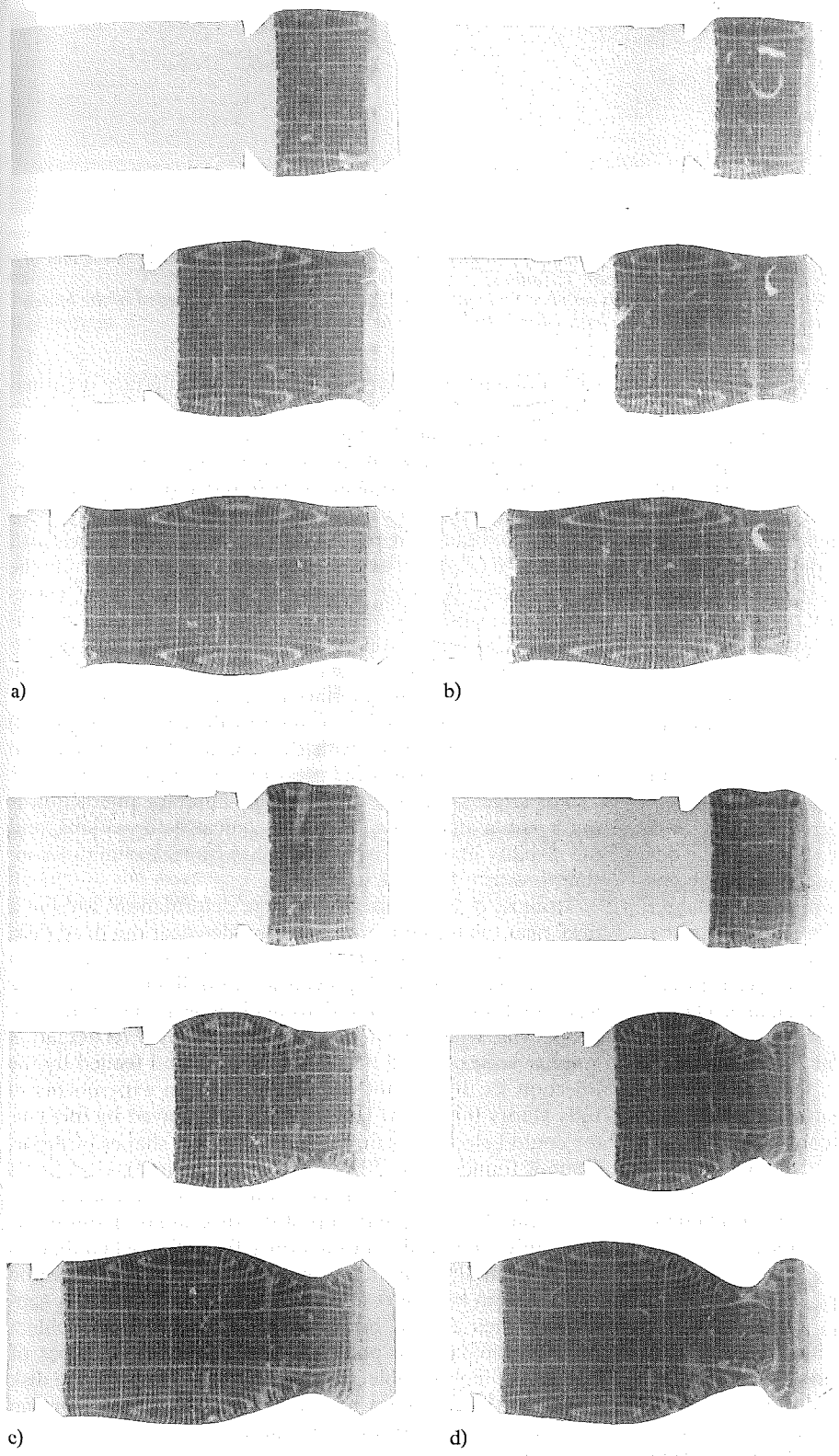

Fig. 9. Pictures of formation processes performed on earth by using the neutral buoyancy technique during some preparation experiments of TEXUS-12 (DMS 5, R_i = 3 mm). Each set of pictures shows three different instants of a formation at constant speed
a) V_d = 2, R = 30; b) V_d = 4, R = 60; c) V_d = 6, R = 90; d) V_d = 8, R = 120. V_d, injection disk speed (mm/s). R, Reynolds number. The double necking of the interface which appears at the largest slendernesses and lowest speeds (2 and 4 mm/s), are mainly due to static effects (stratification of the outer bath). The injection hole is in the moving disk (on the left). $Oh \approx 10^{-2}$

lindrical volume) kept under a constant axial pressure gradient (e.g. residual gravity). Three types of behavior of AB with respect to AC can be observed: $R < 30$, $30 < R < 60$, $R > 60$.

At low Reynolds numbers ($R < 30$) the injection of fluid is just fluid addition without jet formation and the momentum of the fluid is quickly damped by viscous stresses, the perturbation is limited to the neighbourhood of the injection hole (fig. 8a), and therefore the filling process does not influence the stability of the bridge as it is shown in fig. 7, where $\Lambda_c \approx \pi$ for $R < 27$. $\Lambda_c = \pi$ is the static stability limit for unperturbed cylindrical liquid bridges. Concerning expression (2) it is not valid for so small values of R.

In the range $30 < R < 60$ a jet begins to appear and the momentum of the jet is transferred mostly to pressure, and no intense recirculation vortex appears. In these conditions the model developed before makes sense, which is reflected by the remarkable fitting of both stability limits. The direct effect of the jet on the interface is small (low interaction, fig. 8b).

In the case $R > 60$ (high injection speed) the jet produces an intense deformation of the interface giving rise to almost-conical deformations due to a complex pressure distribution with an intense recirculation vortex (fig. 8c). A short bridge can be hardly broken (the heigth of a cone is three times that of the cylinder of equal volume and base) and the breaking is produced by the large deformations generated by the jet. Also there is a measurement error in the breaking position (Λ_c) because the width of the neck can be confused with the jet which impinges in the opposite drop, and the separation of the disks is faster than breaking.

Concerning viscosity effects, its influence is accounted for by the Ohnesorge number. A change in Oh changes the proportion between R and $B^{1/2}$ in (11), and thus, should change the position of the coincident segment of the limit AB ($30 < R < 60$) with the limit AC in fig. 7. It seems that the three above mentioned regions should appear unless R becomes too high for small B. Actually, in some previous experiments performed on earth, in neutral buoyancy, during the preparation of experiment TEXUS-12 (fig. 9) with oil of lower viscosity (DMS 5, $Oh \approx 10^{-2}$), the recirculation vortex near the

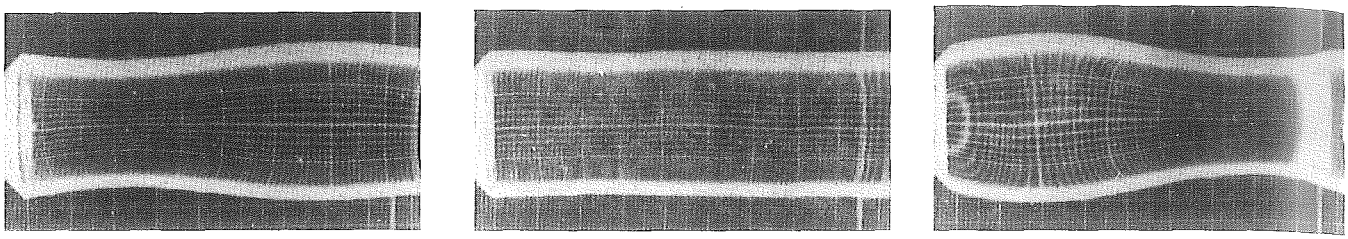

a) b) c)

Fig. 10. Negatives of flight film taken during the experiment (DMS 5, $R_i = 3$ mm), performed onboard TEXUS-12, corresponding to the end of formations of a liquid bridge of 80 mm length at constant disk injection speed. V_d (mm/s)
a) $V_d = 2$, $R = 30$; b) $V_d = 4$, $R = 60$; c) $V_d = 6$, $R = 90$. R, Reynolds number. Only in the last formation, c, the deformation of the bridge continued till the breakage. The injection hole is in the moving disk (on the left). $Oh \approx 10^{-2}$. The outer fluid is air

fixed disk (with clear influence in the interface shape) appearing at $R > 60$ succeeded in inverting the deformation of the interface (producing a neck near the fixed disk, figs. 9b, c and d). The formation of this vortex is related to the penetration of the jet; if the jet does not impinge the opposite disk with enough momentum the vortex does not appear. This phenomenon could clarify the experiment performed in TEXUS-12 [1] in which three different deformations appeared (fig. 10): buldging near the opposite disk (the jet does not reach the disk, $R = 30$, fig. 10a), nearly no deformation (the jet just reaches the disk but the vortex is not strong enough, $R = 60$, fig. 10b), and necking near the opposite disk (the jet impinges the wall, $R = 90$, fig. 10c, the vortex near the opposite disk is strong enough and forces the formation of the neck in its neighbourhood).

If ν_l is small then Oh can be also small. In this way B can be small even if R is large. In these conditions the main effect is the formation of the recirculation vortex near the fixed disk and the jet momentum feeds the vortex directly. The deformation of the bridge would be produced by different mechanisms in this case than in the case of moderately larger Oh, and thus, the limit AB would be different than in the case considered here. Also the meaning of B as deduced from the theoretical model given by expressions (1)–(8) were not longer both applicable and suitable at this smaller Oh.

Unfortunately there were no occasion to perform additional experiment with the low viscosity oil at the appropriate speeds, which could not be reached, as the low viscosity reduced the lubrication of the mechanism, increasing the friction forces and overloading the motor control.

Some trials with tracers were performed at the last sequences due to the damage which they produce in the o-rings. To replace the o-rings the set-up should be dismantled, which could not be made due to time constraints.

5 Conclusions

The formation process of a liquid bridge has been studied. The interest of this process lies in reducing the setting up time of experiments with liquid columns, due to time constraints in performing experiments in space. In first place, some concepts of relevance to this study has been extracted from the literature. A dimensional analysis has been performed which allows to detect the dimensionless parameters of relevance, and a simplified model of the process has been developed valid for $\alpha \ll 1$ (almost-steady evolution) and in a limited range of R and B. The simplified model is based in the assumption that the jet momentum gives rise to a pressure difference between the disks, and the interface deformation is due to this pressure variation.

On the other hand, an experimental study on formation of liquid bridges at several speeds has been performed. The results from these experiments helped to determine the validity range of the theoretical model developed. Thus, in experimental configuration employed ($Oh \approx 4 \cdot 10^{-2}$), for small values of R ($R < 30$) an injection jet does not appear and the liquid bridge stability is not modified by the injection. Therefore, in this case $\Lambda_c \approx \pi$ which is the static result for cylindrical liquid bridges.

In an intermediate range ($30 < R < 60$) a jet appears but its interaction with the interface is small; in this range experimental results (reduced according to the theoretical model) are in good agreement with the stability limit of a liquid bridge under constant axial pressure gradient.

For large values ($R > 60$) the jet-interface interaction is quite strong giving rise to almost-conical deformations, and the stability limit clearly distinguishes from the limit of constant pressure gradient.

In most of these cases the bridge deformations present a neck near the injection disk and a buldge near the fixed disk, as could be expected from the theoretical model. However, in experiments performed previously with liquids of smaller viscosity ($Oh \approx 10^{-2}$) the deformations were just in the opposite way, which seemed to be produced by a recirculation annular vortex placed near the fixed disk and feeded by the injection jet. It was not possible to perform experiments to fully clarify this point. However, the role played by this vortex could help to explain the three different shapes of deformations found in the TEXUS-12 experiments [1].

All the experiments considered here concern quasi-steady evolutions. The start and stop of the disk should require further study. The starting of the bridge formation when there is no bridge at all is an interesting point in itself, and it can be performed in a number of ways. The starting of the disk separation when a short bridge exists is not a major problem from the preparation point of view, because such types of bridges are highly stable. Concerning the stopping of the disk when the final position has been reached, as seen from an observer moving with the injection disk, the flow should be similar to that produced by an imposed abrupt acceleration. The hydrostatic pressure jump across the interface due to this acceleration should be compensated by the interface deformation and the motion of both the inner and the outer fluids. So that the density of the outer fluid has a large influence on the stopping process, and does not seem it can be studied by an straightforward use of the neutral buoyancy

technique, and before a much intense theoretical effort should be provided.

Acknowledgements

The authors want to thank Dr. J. Meseguer and Dr. I. Martínez for their helpful advices. Also they are very indebted to the European Space Agency for the possibility of using the Liquid Column Cell at their Lab, and to the TEXUS project team of ERNO by their technical support in managing the LCC. This study has been partially performed under a contract with SENER from the MINER (Ministerio de Industria y Energía).

References

1. *Martínez, I.* and *Sanz, A.:* Long liquid bridges aboard sounding rockets, ESA Journal 9 (1985), 323–328.
2. *Viilu, A.:* An experimental determination of the minimum Reynolds number for instability in a free jet, J. Appl. Mech. 29 (1962), 506.
3. *Reynolds, A. J.:* Observation of a liquid-into-liquid jet, J. Fluid Mech. 14 (1962), 552.
4. *McNaughton, K. J.* and *Sinclair, C. G.:* Submerged jets in short cylindrical flow-vessels, J. Fluid Mech. 25 (1966), 367.
5. *Taylor, G.:* Low Reynolds-number flows, Film notes, Encyclopaedia Britannica Educational Corporation (1967).
6. *Cantwell, B. J.:* Viscous starting jets, J. Fluid Mech. 173 (1986), 159–189.
7. *Mollendorf, J. C.* and *Gebhart, B.:* An experimental and numerical study of the viscous stability of a round laminar vertical jet with and without thermal buoyancy for symmetric and asymmetric disturbances, J. Fluid Mech. 61 (1973), 367–399.
8. *Deshpande, M. D.* and *Vaishnav, R. N.:* Submerged laminar jet impingement on a plane, J. Fluid Mech. 114 (1982), 213–236.
9. *Meseguer, J.* and *Sanz, A.:* Numerical and experimental study of the dynamics of axisymmetric liquid bridges, J. Fluid Mech. 153 (1985), 83–101.
10. *Sanz, A.:* The influence of the outer bath in the dynamics of axisymmetric liquid bridges, J. Fluid Mech. 156 (1985), 101–140.
11. *Sanz, A.* and *Martínez, I.:* Minimum volume for a liquid bridge between equal disks, J. Colloid Interface Sci. 93 (1983), 235–240.

List of Symbols

B	Bond number, $B = \Delta p\, R_0/(2\, \Lambda\, \sigma)$
$C(z)$	Mean curvature of the interface
D	Penetration of a jet in a surrounding fluid
$F(z,t)$	Shape of the interface
F_s	Axial force of the interface over the liquid
L	Disk separation
Oh	Ohnesorge number, $Oh = \nu_i(\sigma\, R_0/\varrho_i)^{-1/2}$
R	Reynolds number, $R = 2\, R_i\, V_i/\nu_i$
R_c	Reynolds number used in [6]
R_i	Injection radius
R_0	Disk radius
St	Strouhal number, $St = t_r/t_c$
T	Dimensionless time, $T = t/t_c$
V_d	Disk separation speed
V_i	Mean injection speed
W	Weber number, $W = \varrho_i\, V_d^2\, R_0/\sigma$
Z	Dimensionless axial coordinate, $Z = z/R_0$
Z_m	Dimensionless axial coordinate of maximum f
f	Dimensionless interface deformation, $f = F/R_0 - 1$
f_m	Maximum dimensionless interface deformation
k	Matching factor
$p_i(z)$	Pressure inside the liquid bridge
p_0	Pressure outside the liquid bridge
Δp	Pressure difference between the disks
r	Radial coordinate
t	Dimensional time
t_c	Characteristic time, $t_c = L/V_d$
t_r	Residence time, $t_r = L/V_i$
z	Axial coordinate
Λ	Slenderness of the liquid bridge, $\Lambda = L/(2\, R_0)$
Λ_c	Critical slenderness
α	Radius ratio, $\alpha = R_i/R_0$
ν	Viscosity ratio, $\nu = \nu_0/\nu_i$
ν_i	Kinematic viscosity of the bridge liquid
ν_0	Kinematic viscosity of the surrounding bridge
ϱ	Density ratio, $\varrho = \varrho_0/\varrho_i$
ϱ_i	Bridge liquid density
ϱ_0	Surrounding liquid density
σ	Interface tension
θ	Angle of the interface slope with the z axis